



28

29 Submitted to Carbohydrate Polymers, August, 2016

30 Revised, October 2016

31

32

33

34 **Abstract**

35 Thermoplastic starch (TPS) biocomposites modified with cellulose microfibrils and/or  
36 natural rubber were prepared via extrusion compounding. Glycerol and water served  
37 as plasticizers for starch. The dielectric properties of the TPS composites were  
38 examined via broadband dielectric spectroscopy in the temperature and frequency  
39 ranges of 30°C to 65°C and 0.1 Hz to 10 MHz, respectively. Each specimen was  
40 tested twice in order to study the effect of absorbed water. The  
41 hydrophobic/hydrophilic character of the modifiers governed the dielectric  
42 performance of the corresponding TPS biocomposites. Conducted analysis revealed  
43 two relaxation processes attributed to matrix-water-reinforcement interfacial  
44 polarization and glass to rubber transition of the TPS. Evaporation of water  
45 significantly affected the first process and only slightly the second one. Energy  
46 density, prior and after water evaporation, was also determined at constant field. By  
47 employing dielectric reinforcing function the contributions of water-assisted and  
48 constituents' originated interfacial phenomena could be separated.

49

50

51 Key words: thermoplastic starch, microfibrillar cellulose, natural rubber latex,

52 broadband dielectric spectroscopy, water effect

53

54

55

56

57

## 58 **1. Introduction**

59 In the past few decades, considerable scientific interest was focused to  
60 biodegradable, ecologically friendly polymers produced from renewable resources.  
61 The development of agro-based biopolymers aims at replacing less environmentally  
62 benign synthetic polymers in a variety of applications, mostly in packaging industry  
63 (Bugnicourt, Cinelli, Lazzeri, & Alvarez, 2014; Chung et al., 2010; Lendvai, Karger-  
64 Kocsis, Kmetty, & Drakopoulos, 2016; Nafchi, Moradpour, Saeidi, & Alias, 2013;  
65 Tábi, & Kovács, 2007).

66 One of the most studied biobased polymer is starch, which can be found in potato,  
67 corn, rice, pea and other plants. Starch is abundant in nature, inexpensive and most  
68 importantly, biodegradable (Chung et al., 2010; Kamel, 2007; Nasser, &  
69 Mohammadi, 2014). Starch is a polysaccharide consisting of two distinct substances  
70 of d-glucose units; amylose which is a linear macromolecule in helical three-  
71 dimensional form and amylopectin which is a branched biopolymer. Starch exhibits  
72 no thermoplastic behavior, although it can be altered to thermoplastic after suitable  
73 processing, using mechanical shear and heating in presence of suitable plasticizers  
74 (Majdzadeh-Ardakani, Navarchian, & Sadeghi, 2010; Xie, Pollet, Halley, & Avérous,  
75 2013). **The most prominent application of thermoplastic starch, at the moment, is its  
76 potential to replace synthetic polymers in packaging industry as it is completely  
77 biodegradable in water and soil (Chen & Evans, 2005; Majdzadeh-Ardakani, et al.,**

78 2010). In addition, applications in biomedical engineering and biomedicine can also  
79 be found as TPS (sometimes with the addition of another polymer to form a polymer  
80 blend) has been suggested to be suitable as scaffold materials in bone tissue  
81 engineering and as a carrier for controlled drug release (Mano, Koniarova, & Reis,  
82 2003).

83 Various plasticizers can be used into thermoplastic starch (TPS) like, sorbitol,  
84 glycerol and water. The amount of plasticizer employed in the mixture is critical for  
85 the mechanical and thermal properties, such as Young's modulus and glass to rubber  
86 transition respectively (Dean, Yu, & Wu, 2007; Karger-Kocsis, Kmetty, Lendvai,  
87 Drakopoulos, & Bárány, 2015; Kmetty, Karger-Kocsis, & Czigány, 2015; Liu, Xie,  
88 Yu, Chen, & Li, 2009; Schlemmer, Angélica, & Sales, 2010). Water can act also as a  
89 plasticizer when is added in starch granules. In fact, starch granules swell when water  
90 is added due to H-bonding between water and hydroxyl side groups of the main  
91 polymeric chain. Under the influence of mechanical shear and heat, starch becomes  
92 gelatinized starch (Lendvai et al., 2016). However, plasticized starch-based materials  
93 face humidity and temperature problems, meaning that fundamental properties like  
94 mechanical and thermal performance are highly affected. Hence, suitable reinforcing  
95 materials and modifiers need to be employed in order to enhance further these  
96 properties (Xie, et al., 2013).

97 One of the most efficient methods for melt compounding of thermoplastic polymers  
98 is the extrusion technique. Single- or twin-screw extruders are usually used for  
99 manufacturing polymer blends or/and reinforced polymers (Nafchi et al., 2013;  
100 Ruellan et al., 2015; Xie et al., 2013), including TPS-based ones.

101 Broadband Dielectric Spectroscopy (BDS) is a powerful tool for studying  
102 molecular mobility, conductivity and interfacial effects in polymers and composite

103 materials (Kremer & Schönhals, 2009). Dielectric measurements have been used for  
104 the characterization of relaxation processes in biobased composite materials (Arous,  
105 Ben Amor, Boufi, & Kallel, 2007; Ladhar et al., 2014).

106 Natural rubber (NR) is used as an engineering material for many years, both as a  
107 matrix and as modifier (Ortiz-Serna, Carsí, Redondo-Foj, & Sanchis, 2014;  
108 Siengchin, Karger-Kocsis, & Thomann, 2008). NR is a hydrophobic, non-polar,  
109 insulating material which is mainly derived from the latex of *Hevea brasiliensis* or  
110 Hevea Rubber tree (Gatos, Martínez Alcázar, Psarras, Thomann, & Karger-Kocsis,  
111 2007; Psarras et al., 2007; Psarras, Gatos, & Karger-Kocsis, 2007; Rolere, Bottier,  
112 Vaysse, Sainte-Beuve, & Bonfils, 2016; Rose, & Steinbüchel, 2005; Siengchin,  
113 Karger-Kocsis, Psarras, & Thomann, 2008; Tanrattanakul, & Bunkaew, 2014).

114 Cellulose consisting of D-glucose units is a hydrophilic linear  
115 biomacromolecule with promising biodegradable and reinforcing properties (Ladhar  
116 et al., 2014; Ortiz-Serna et al., 2014). To achieve the latter, however, its microfibrillar  
117 (micronscale) or whisker (nanoscale) versions are preferred. Cellulose is also a  
118 promising reinforcement in biomedical engineering applications due to its  
119 biocompatibility (Iqbal, Kyazze, Locke, Tron, & Keshavarz, 2015). **In medicine,**  
120 **natural rubber latex has been investigated for over 100 years on enhancing it upon**  
121 **biodegradation from fungi and bacteria, in order to product gloves and other medical**  
122 **equipment (Rose & Steinbüchel, 2005). Additionally, biomedical engineering**  
123 **applications employ natural rubber latex membranes as protein delivery systems in**  
124 **guided bone regeneration. These membranes follow a modified manufacturing**  
125 **process producing a much better biocompatible polymer (Herculano, et al., 2009).**

126 In the present study, TPS biocomposites modified with microfibrillated cellulose  
127 and/or NR microparticles were prepared. The dielectric properties of the produced

128 biocomposites were investigated by means of BDS in the frequency range of  $10^{-1}$  to  
129  $10^6$  Hz and temperatures varying from 30 to 65°C. Each specimen was tested twice in  
130 the same frequency-temperature profile, in order to clarify the effect of the absorbed  
131 water, and to study the influence of the hydrophilic/hydrophobic character of the  
132 employed modifiers. The latter is related to interfacial phenomena between the  
133 constituents of the composites and is connected with their ability to store energy.

134

## 135 **2. Experimental**

### 136 *2.1. Materials*

137 Commercially available native corn starch (CS) Hungramid F Meritena 100  
138 (obtained from Brennrag Ltd., Budapest, Hungary) was used as matrix material. As  
139 plasticizers, were used glycerol (purity of 99.5% purchased from Csepp Bt., Budapest,  
140 Hungary) and distilled water. Two types of modifiers were introduced, the  
141 microfibrillated cellulose (referred to as B600): Arbocel® B 600 with average length  
142 of 60  $\mu\text{m}$ , diameter of 20  $\mu\text{m}$  (JRS GmbH, Rosenberg, Germany) and NR latex  
143 (denoted as Latex further on) particles: (dry content of the NR latex 60%, supplied by  
144 Varicham Ltd., Hungary). Stearic acid (purchased from ICC-Chemol Ltd., Budapest,  
145 Hungary) was used as lubricant for thermoplastic starch.

146 The corn starch, microfibrillated cellulose and stearic acid powders were  
147 conditioned in a Memmert HCP153 (Frankfurt, Germany) humidification chamber at  
148 30°C and relative humidity of 50% for at least 168 hours prior to processing in order  
149 to have the same moisture content during the specimens preparation.

150

### 151 *2.2. Methods*

152 A premix was prepared which included a manual mixing of starch, plasticizers,  
 153 lubricant and either microfibrillated cellulose or latex or both. The ratio of  
 154 starch/glycerol was fixed to exactly 4:1 wt/wt in every mixture. The composition of  
 155 all mixtures is indicated in Table 1. Additionally, in every mixture, 20 g water was  
 156 added for every 100 g of premix (not included in Table 1). Also, 1wt % stearic acid  
 157 was added as lubricant in order to avoid high pressure during the extrusion (Tábi, &  
 158 Kovács, 2007).

159

160 **Table 1:** Composition of all employed mixtures after extrusion and samples mass  
 161 difference prior and after the first thermal cycle.

Sample	Starch (wt %)	Glycerol (wt %)	MFC (wt %)	Latex (wt %)	$\Delta m$ (g)
TPS	80	20	-	-	0.008
TPS+10% B600	72	18	10	-	0.006
TPS+20% B600	64	16	20	-	0.007
TPS+10% Latex	72	18	-	10	0.010
TPS+20% Latex	64	16	-	20	0.006
TPS+10% B600+10% Latex	64	16	10	10	0.007
TPS+20% B600+10% Latex	56	14	20	10	0.008

162

163 Furthermore, the premix in every mixture was melt-compounded using a twin-  
 164 screw extruder (LTE 26-44, Labtech Engineering, Samut Prakarn, Thailand) with an  
 165 L/D ratio of 44 and screw diameter of 26 mm. The screw velocity was 75 rpm and  
 166 contained 11 heating zones (including the die) where the temperature was 85, 90, 95,  
 167 100, 100, 100, 110, 110, 120 and 120°C, while the temperature of the die was also

168 120°C. Premix was manually transported to the extruder. The extruder had also an  
169 atmospheric vent to remove the vaporized water (at heating zone 7). After the  
170 extrusion, the pellets were conditioned again for a week and then were compression  
171 molded to sheets of 1.7 mm average thickness with a hot press machine (Teach-Line  
172 Platen Press 200E, Dr. Collin GmbH, Munich, Germany) at temperature 130°C for 2  
173 minutes and pressure 100 bars. Specimens for testing were cut of the compression  
174 molded sheets (Ledvai et al., 2016). *After their preparation, specimens were stored in  
175 small plastic bags at room temperature for short time before testing, in order to avoid  
176 the effect of any biodegradation.*

177

### 178 *2.3. Broadband dielectric spectroscopy*

179 The electrical response of the prepared systems was investigated by means of BDS  
180 using an Alpha-N Frequency Response Analyzer, provided by Novocontrol  
181 Technologies (Hundsagen, Germany). The voltage amplitude of the applied field was  
182 kept constant at 1 V, while frequency varied from  $10^{-1}$  to  $10^6$  Hz. Isothermal scans  
183 were conducted in the temperature range from 30 to 65°C, in steps of 5°C. *The  
184 employed temperature range was selected, after relative tests, in order to determine  
185 conditions where no irreversible alteration, of the examined composites, will occur.*  
186 Temperature was controlled via the Novotherm system and the dielectric test cell used  
187 was the BDS-1200, parallel-plate capacitor, with two gold-plated electrodes system,  
188 all supplied by Novocontrol. *Dielectric cell was kept in dry conditions prior each test  
189 in order to avoid the influence of possible humidity.*

190 Each specimen was subjected to two identical and successive thermal cycles. The  
191 variation of specimens mass prior and after the first thermal cycle is shown in Table 1.

192



193 **3. Results and Discussion**

194 *3.1. Dielectric response-effect of water molecules*

195 The dielectric response of all mixtures is shown in Figs 1 and 2. Dielectric data are  
196 presented in terms of dielectric permittivity and electric modulus formalisms.  
197 Complex dielectric permittivity and electric modulus are defined according to  
198 Equations (1) and (2):

199 
$$\varepsilon^* = \varepsilon' - i\varepsilon'' \quad (1)$$

200 
$$M^* = \frac{1}{\varepsilon^*} = \frac{1}{\varepsilon' - i\varepsilon''} = \frac{\varepsilon'}{\varepsilon'^2 + \varepsilon''^2} + i \frac{\varepsilon''}{\varepsilon'^2 + \varepsilon''^2} = M' + iM'' \quad (2)$$

201

202 where,  $\varepsilon'$ ,  $\varepsilon''$  and  $M'$ ,  $M''$  are the real and the imaginary parts of dielectric  
203 permittivity and electric modulus respectively. Arguments for the advantages of  
204 analyzing dielectric data in terms of different formalisms have been discussed  
205 elsewhere (Tsangaris, Psarras, & Kouloumbi, 1998).

206 Fig. 1 depicts the variation of the real part of dielectric permittivity as a function of  
207 temperature before and after water evaporation (1<sup>st</sup> -Figs 1a,c- and 2<sup>nd</sup> -Figs 1b,d-  
208 thermal cycle respectively) at  $10^3$  and  $10^6$  Hz (Figs 1a,b and 1c,d).

209

210

211

212

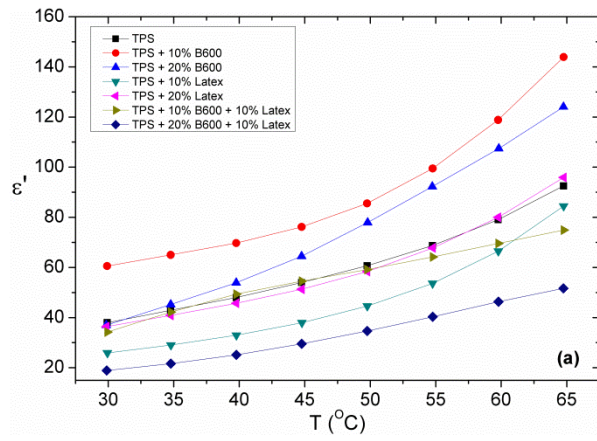
213

214

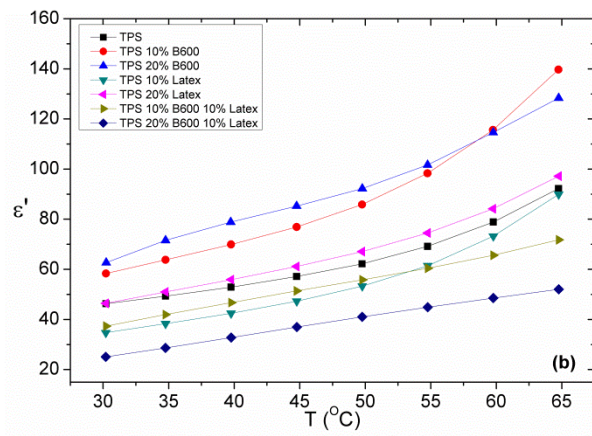
215

216

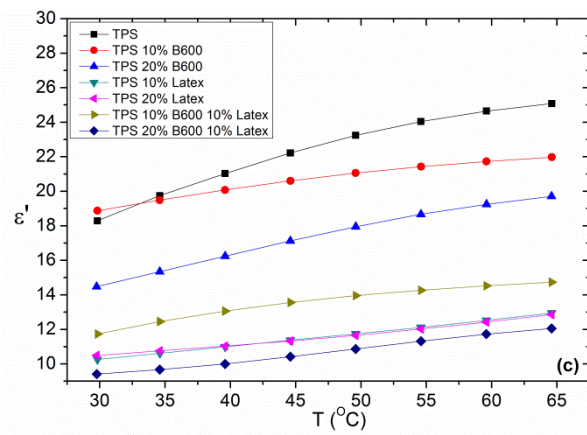
217



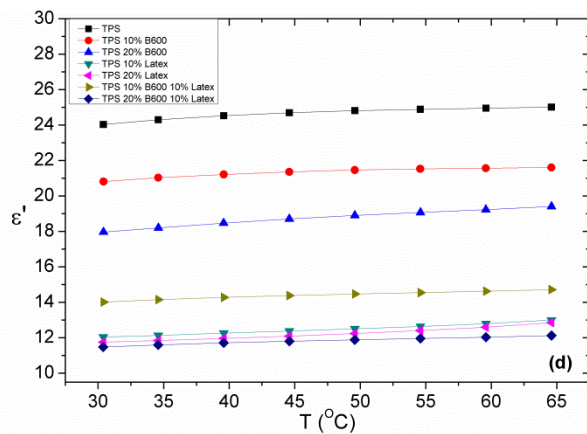
218



219



220



221 **Fig. 1:** The real part of dielectric permittivity as a function of temperature for all  
222 specimens at: (a)  $10^3$  Hz, first thermal cycle, (b)  $10^3$  Hz, second thermal cycle, (c)  $10^6$   
223 Hz, first thermal cycle and (d)  $10^6$  Hz, second thermal cycle.

224

225 Polarization and  $\epsilon'$  attain high values at low frequencies since permanent and induced  
226 dipoles acquire sufficient time to be aligned parallel to the field (Figs 1a and b).

227 Dipoles orientation is a thermally assisted process and thus permittivity increases, in  
228 general, with temperature. In Fig. 1a and Fig. 1b it can be seen that the cellulose

229 reinforced composites exhibit the highest values of  $\epsilon'$  throughout the whole  
230 temperature spectrum at  $10^3$  Hz. As both cellulose and starch (amylose and

231 amylopectin) consist of glucose units (which have four hydroxyl groups and a  
232 methylol group (-CH<sub>2</sub>OH) linked to the main chain), they have very similar chemical

233 formulae but different three-dimensional structures. Since cellulose is a linear  
234 macromolecule, it is easier to be aligned with the applied electric field than amylose

235 and amylopectin, resulting thus to higher values of polarization and  $\epsilon'$  (Fig. 1a).

236 Cellulose and amylose are hydrophilic molecules due to the high concentrations of  
237 hydroxyl groups and their 3D form. As cellulose is a linear macromolecule and

238 amylose is quasi-linear in a helical form, they exhibit differences in their hydrophilic  
239 behavior. In the case of amylose, less hydroxyl groups are participating in the

240 intramolecular hydrogen bonds with water molecules, and as such, it is less  
241 hydrophilic than cellulose. The enhanced hydrophilic character of cellulose results in

242 the attraction of water molecules, causing an obstruction to the motion of the polymer  
243 chains. It should be considered that cellulose is a semi-crystalline polymer and its

244 crystallinity could exert restrictions to cellulosic chains mobility. Crystalline regions,  
245 in semi-crystalline polymers, typically constrain amorphous parts of the polymer, due

246 to their rigidity leading to higher values of glass to rubber transition temperature.  
247 Enhancement of  $T_g$  with the increase of cellulose (B600) has been confirmed via  
248 DMTA tests in a previous work (Lendvai et al., 2016). However, the presence of  
249 cellulose in the hybrid composites, in the same tests, didn't lead to an increase of  $T_g$ ,  
250 indicating that the presence of interfaces allows hydrophilicity to have a stronger  
251 effect upon the resulting electrical polarization. Moreover, amorphous parts, because  
252 of the absence of long range order, might favor the water penetration between chains  
253 and thus the interactions, which result in the formation of H-bonds. So, the effect of  
254 cellulose crystallinity in the relative systems is not considered as predominant.

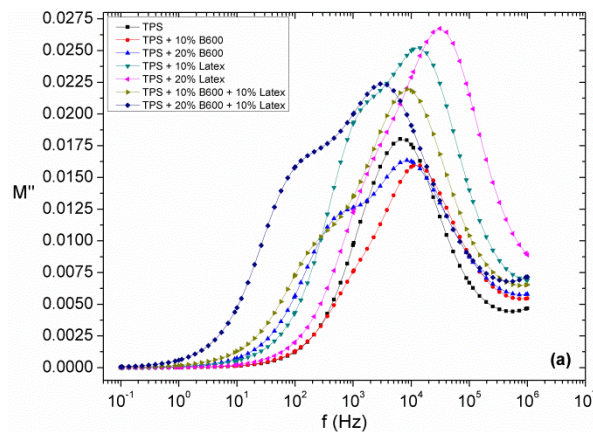
255 Hence, although cellulose is aligned easier with the electric field than starch, higher  
256 cellulose concentrations attract more water molecules leading to a hindrance of the  
257 polar groups' orientation. Thus, the 10% B600 reinforced specimen attains higher  
258 values of  $\epsilon'$  compared to the 20% B600 sample. On the other hand, NR (latex) is a  
259 hydrophobic non polar material exhibiting lower values of dielectric permittivity than  
260 the TPS matrix (Psarras et al., 2007). In the NR latex modified composites two  
261 competitive procedures are present. The significantly lower values of  $\epsilon'$  for NR  
262 compared to TPS lead to a decrement of the overall permittivity of the corresponding  
263 composites. On the other hand, with increasing the latex concentration the  
264 hydrophobic character of the composites becomes more prominent. Thus, the density  
265 of H-bonds, and consequently the exerted obstructions to the orientation of the starch  
266 macromolecules parallel to the electric field diminish. As a result the presence of 10%  
267 latex in TPS matrix causes an initial reduction of dielectric permittivity, due to its low  
268 values, which is countered back with the increase of latex content (20% latex),  
269 because of the facilitation of system's polar groups to be oriented with the applied  
270 field. Thus the reduction of H-bonds leads to a secondary increase of  $\epsilon'$  (Fig. 1a).

271 In the case of the hybrid (i.e. microfibrillated cellulose + NR latex) composites low  $\epsilon'$   
272 values have been observed, and all the above mentioned influences are active. It is  
273 believed that due to higher concentrations of both modifiers more water is trapped  
274 between the TPS matrix and the cellulose reinforcement yielding enhanced interfacial  
275 interactions. When water molecules are near to amylose or cellulose macromolecules,  
276 H-bonds are formed causing an obstruction to the movement of polar groups with the  
277 applied electric field. Between the first and the second thermal cycle, Fig. 1a and 1b  
278 respectively, an increase in  $\epsilon'$  has been observed only in temperatures up to 50°C due  
279 to water evaporation. At higher temperatures, after water removal, no significant  
280 difference has been observed between the first and second cycles. In Fig. 1c and 1d,  
281 the highest values of  $\epsilon'$  belong to starch macromolecules. In this frequency ( $10^6$  Hz) a  
282 secondary and weaker polarization effect occurs due to the orientation of smaller  
283 polar segments, like free hydroxyl groups (not forming H-bonds). Although starch  
284 and cellulose possess equal number of hydroxyl groups, they differ in the number of  
285 the formed H-bonds between hydroxyl groups and water molecules, as mentioned  
286 previously. Amylose and amylopectin contain a greater amount of free hydroxyl  
287 groups than cellulose and as such, TPS exhibits higher values of  $\epsilon'$  than the cellulose  
288 reinforced composites. Latex modified TPS and the hybrids exhibit lower  $\epsilon'$  values as  
289 latex contains no hydroxyl groups at all and is a low permittivity material. At  $10^6$  Hz,  
290 the difference in  $\epsilon'$  values between the first and second thermal cycle, is more intense  
291 at temperatures below 50°C, as in the case of  $10^3$  Hz.

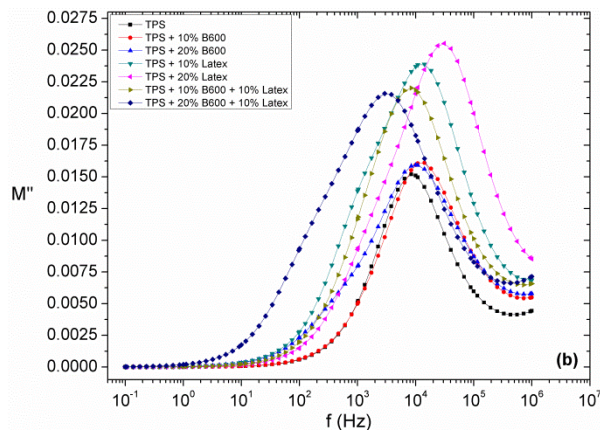
292

293 Fig. 2a presents the dependence of the imaginary part of electric modulus ( $M''$ ) upon  
294 frequency at 30°C for the first thermal cycle. The loss index of electric modulus forms  
295 a peak at medium to high frequencies, in all examined samples, which is attributed to

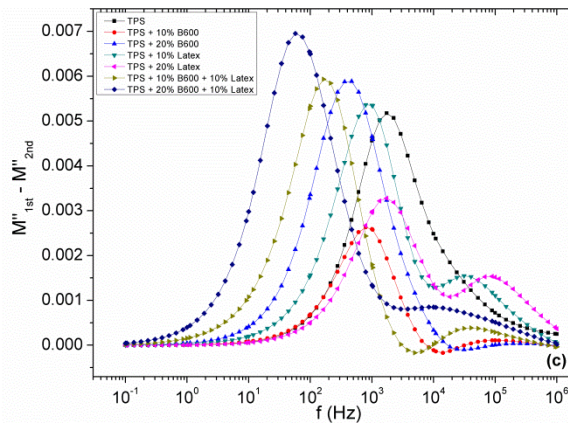
296 the glass to rubber transition of the polymer matrix, also noted as  $\alpha$ -relaxation. A  
 297 shoulder also appears at relatively lower frequencies, in the intermediate frequency  
 298 range, which is attributed to a matrix-water-reinforcement interfacial polarization  
 299 (MWR-IP). Water molecules lie in the interface between TPS and cellulose, where  
 300 unbounded charges are also present. Thus, the resulting interfacial phenomena are  
 301 related to dipole-dipole and dipole-charge interactions. Consequently, H-bonds are  
 302 formed between the hydroxyl groups of glucose units of both starch and cellulose  
 303 macromolecules. This phenomenon languishes as the temperature rises until most of  
 304 the water is evaporated. The latter is clear in Fig. 2b which shows the imaginary part  
 305 of electric modulus at 30°C for the second thermal cycle, where no MWR-IP is  
 306 observed and only the peak of  $\alpha$ -relaxation is recorded. From Fig. 2a it is obvious that  
 307 MWR-IP is characterized by a longer relaxation time, compared to  $\alpha$ -relaxation, since  
 308 it is recorded at lower frequencies.



309



310



311

312 **Fig. 2:** The imaginary part of electric modulus for all specimens as a function of  
 313 frequency at 30°C, for the: (a) first, (b) second thermal cycle, and (c) spectra  
 314 subtraction between the first the second thermal cycle.

315

316 Fig 2c depicts the subtraction of the loss modulus spectra prior and after water  
 317 removal (i.e. the “dry” spectra of Fig. 2b are subtracted from the corresponding  
 318 spectra of Fig. 2a). It is reasonable to consider that the remaining spectra of Fig. 2c  
 319 represent the contribution of water. The recorded processes appear to be weaker than  
 320 those present in the spectra of the first and the second cycle, and the main peak is  
 321 recorded very close to the frequency range where the MWR-IP shoulders are observed  
 322 in the loss curves of the first thermal cycle. Interestingly another relaxation process is  
 323 present, in the spectra of Fig. 2c, at the high frequency edge. This process appears to  
 324 be more intense in the case of the composites modified with the hydrophobic NR  
 325 latex, while is significantly weaker in the case of the hydrophilic cellulose reinforced  
 326 composites. The same process in hybrid composites exhibits an intermediate and  
 327 rather broad performance, since both hydrophilic and hydrophobic reinforcements co-  
 328 exist. The physical origin of this dielectric process could be ascribed to the polarity of  
 329 unbounded or free water molecules. Unlike hydrophilic inclusions, hydrophobic  
 330 fillers favor the presence of unbounded water molecules and thus the onset of the

331 corresponding dielectric process. The intermediate behavior of hybrid composites  
332 supports the previous interpretation since it can be considered as the superposition of  
333 two influences acting at opposite directions. This process although it should be  
334 present in the spectra of Fig. 2a, prior of water removal, it is hidden under the stronger  
335 effect of  $\alpha$ -relaxation.

336 DSC thermographs (not shown here) recorded under two identical thermal cycles with  
337 the BDS tests indicate the evaporation of water upon heating in the first run, although  
338 no evidence for the initial location (interface or matrix) of water could be extracted.

339

### 340 3.2. Molecular dynamics

341 Fig. 3 shows the loss peak positions of the observed relaxation phenomena as a  
342 function of reciprocal temperature, prior and after water evaporation (i.e. first and  
343 second cycle, respectively). Fig. 3a presents the loss peak positions of both  $\alpha$ -  
344 relaxation and MWR-IP. MWR-IP is easily observed only up to 45°C, because of  
345 water evaporation. Matrix-water-cellulose reinforcement interfacial polarization and  
346 Maxwell-Wagner-Sillars effect exhibit a set of common characteristics including  
347 longer relaxation time than the  $\alpha$ -mode, Arrhenius temperature dependence and  
348 relation to interfacial phenomena. The loss peak positions after water evaporation  
349 (second thermal cycle) are depicted in Fig. 3b, where only  $\alpha$ -relaxation is observed.

350 The temperature dependence of the MWR-IP peaks maxima can be described by the  
351 Arrhenius relation (cf. Equation 3):

352

$$353 f_{max} = f_0 e^{-\frac{E_A}{k_B T}} \quad (3)$$

354



355 where  $f_0$  is a pre-exponential factor,  $E_A$  is the activation energy,  $k_B$  the Boltzmann  
356 constant and  $T$  the absolute temperature. On the other hand, the temperature  
357 dependence of  $\alpha$ -relaxation obeys the Vogel-Fulcher-Tammann (VFT) relation – cf.  
358 Equation 4:

359

$$360 \quad f_{max} = f_0 e^{-\frac{AT_0}{(T-T_0)}} \quad (4)$$

361

362 where  $f_0$  is a pre-exponential factor,  $A$  a constant being the measure of activation  
363 energy,  $T_0$  the Vogel temperature or ideal glass transition temperature and  $T$  the  
364 absolute temperature. The fitting parameters of Arrhenius and VFT equations to the  
365 experimental data are given in Table 2. It should be noted, that recorded data did not  
366 lead to reliable fittings for the MWR-IP process in all specimens. These cases are  
367 omitted from both Fig. 3 and Table 2.

368

369

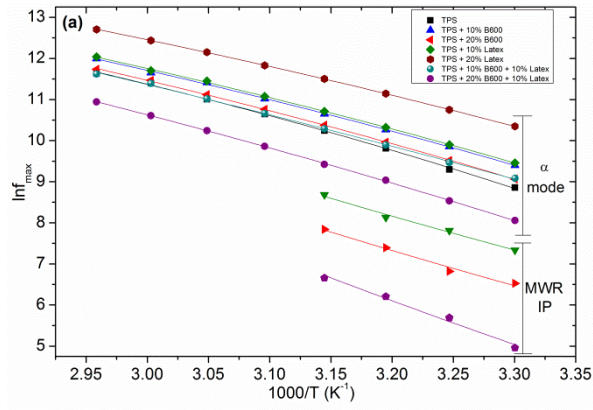
370

371

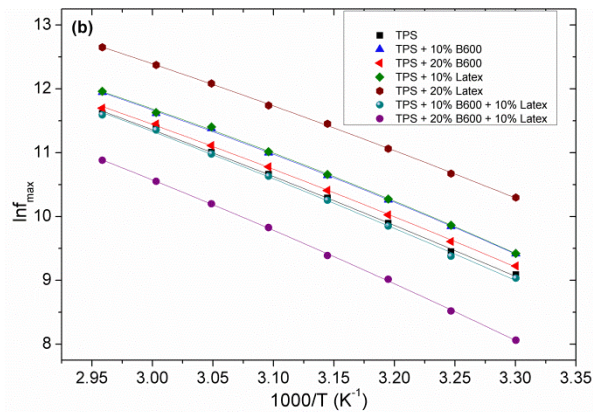
372

373

374



375



376

377 **Fig. 3:** Loss peak position of the recorded relaxations, as a function of reciprocal  
 378 temperature for the: (a) first and (b) second thermal cycle.

379

380 **Table 2:** Activation energy for matrix-water-reinforcement-interfacial polarization  
 381 and Vogel parameters for  $\alpha$ -relaxation for both thermal cycles.

382

383

384

385

386

387

388

Specimen	MWR-IP	$\alpha$ -mode			
		1 <sup>st</sup> cycle		2 <sup>nd</sup> cycle	
	$E_A$ (eV)	A	$T_0$ (K)	A	$T_0$ (K)
TPS	-	0.240	234.62	0.437	207.01
TPS+10% B600	-	0.287	223.00	0.285	222.39
TPS+20% B600	0.780	0.276	227.09	0.371	212.27
TPS+10% Latex	0.750	0.279	223.64	0.264	225.43
TPS+20% Latex	-	0.278	217.55	0.352	207.99
TPS+10% B600+ 10% Latex	-	0.446	206.14	0.422	209.41
TPS+20% B600+ 10% Latex	0.949	0.351	224.14	0.360	222.48

389

390 VFT parameters are highly affected when the evaporated water molecules were acting  
391 as plasticizing agents. Thus, the stronger effect is observed in the case of the TPS  
392 sample.  $T_0$  values shift to lower values, as expected, with the evaporation of  
393 plasticizing water molecules, since the TPS polymer chains achieve increased  
394 mobility, because of the reduction of restricting the H-bonds, and the relative  
395 relaxation process is facilitated. The same trend has been observed in the actual  $T_g$   
396 value of the systems, as determined via DMTA studies (Lendvai et al., 2016). The  
397 variations of parameter  $A$  are in accordance with those of  $T_0$ , since parameter  $A$   
398 reflects the required amount of activation energy for the glass to rubber transition  
399 process.

400 Values of activation energy  $E_A$  for the MWR-IP process are higher in the case of  
401 TPS/cellulose composites than in the case of TPS/latex ones, since cellulose is

402 hydrophilic and latex is hydrophobic and thus water molecules are stronger bonded at  
403 the interface in the first case. Notably, the system with the highest heterogeneity  
404 (TPS+20% B600+ 10% Latex) exhibits the highest value of  $E_A$ . Trapped water  
405 molecules between the interfaces of the constituents restricted by the interactions with  
406 cellulose and amylose, and their ability to be polarized with the field diminishes.

407

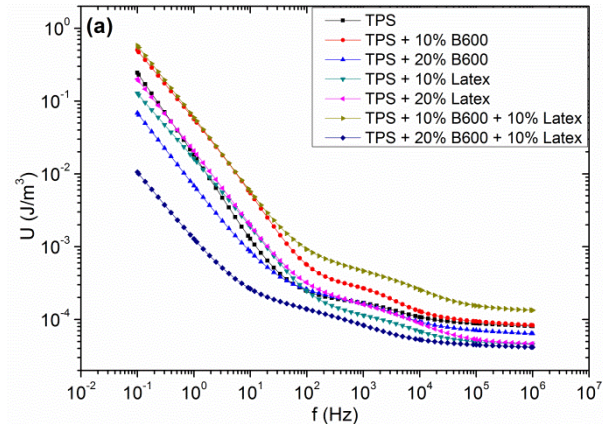
### 408 3.3. Energy density and dielectric reinforcing function

409 Fig. 4 presents the energy density and the normalized energy density as a function  
410 of frequency for all specimens at constant electric field  $E = 1$  kV/m, at 30°C. Energy  
411 density is defined via Equation (5), as follows:

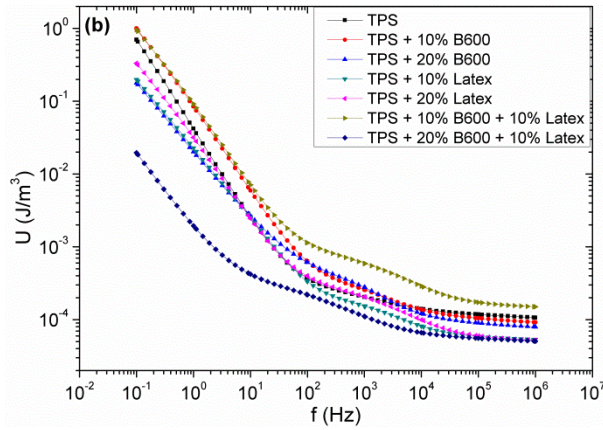
$$412 \quad U = \frac{1}{2} \varepsilon_0 \varepsilon' E^2 \quad (5)$$

413 where  $\varepsilon_0$  is the permittivity of free space and  $E$  the intensity of the applied electric  
414 field. From Equation (5) it is apparent that energy density is highly affected by the  
415 electric field, being also limited by its maximum value at the dielectric breakdown.  
416 However, the only material property influencing energy density is the real part of  
417 dielectric permittivity.

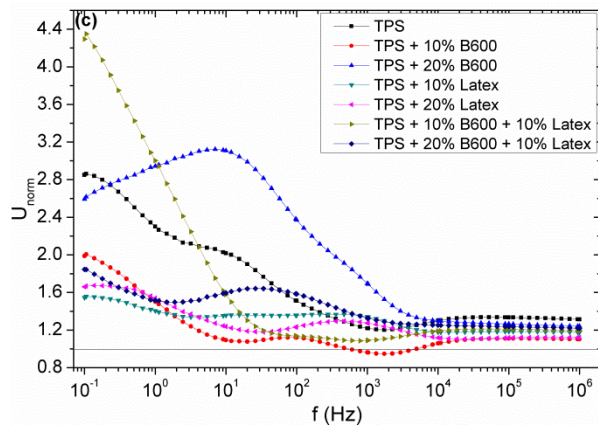
418



419



420



421 **Fig. 4:** Energy density as a function of frequency for all specimens at constant electric  
 422 field  $E = 1 \text{ kV/m}$  at  $30^\circ\text{C}$ , (a) prior and (b) after water evaporation. (c) Normalized  
 423 energy density as a function of frequency for all specimens.

424

425 Normalized energy density is defined according to Equation (6):

426

427 
$$U_{norm} = \frac{U_{2nd}}{U_{1st}} \quad (6)$$

428

429 where  $U_{2nd}$  and  $U_{1st}$  are the values of energy density for the second and first thermal  
430 cycle, respectively.

431 Fig. 4a presents the energy density for the first thermal cycle while Fig. 4b for the  
432 second one. As expected, energy density at constant field follows the variation of  $\epsilon'$   
433 and at low frequencies it attains high values. In medium frequency range,  $\epsilon'$  values are  
434 less dependent on frequency until they reach almost constant values at the high  
435 frequency edge. Step-like transitions from high to low values of energy density at  
436 intermediate frequencies imply the role of  $\alpha$ -relaxation process. From both Fig. 4a and  
437 4b, it is evident that the specimens with the lowest energy density values are those  
438 with the most intense presence of MWR-IP (cf. Fig 3). This is attributed to the intra-  
439 molecular hydrogen bonds formed between water molecules and hydroxyl group of  
440 the TPS chain and as a result reduces polarization and thus  $\epsilon'$ . On the other hand, the  
441 specimens of TPS + 10% B600 and TPS + 10% B600 + 10% Latex which had  
442 relatively low water concentration (Fig. 2a), exhibit the highest values, rising up to 1  
443  $J/m^3$  at  $10^{-1}$  Hz. Furthermore the TPS energy density seems not to be affected by the  
444 presence of latex modification. Fig. 4c shows that all specimens after water  
445 evaporation exhibit 1.5 to 4.4 times higher values of energy density at low frequencies  
446 at 30°C. Evaporation of water minimizes the hydrogen bonds between water  
447 molecules and hydroxyl side groups of the main polymer chains, and thus reduces the  
448 exerted mobility restrictions. Hence, system's polarization becomes easier since polar  
449 groups are facilitated in their alignment to the field and therefore the real part of  
450 dielectric permittivity gets higher values.

451 Dielectric Reinforcing Function (DRF) is defined according to Equation (7):

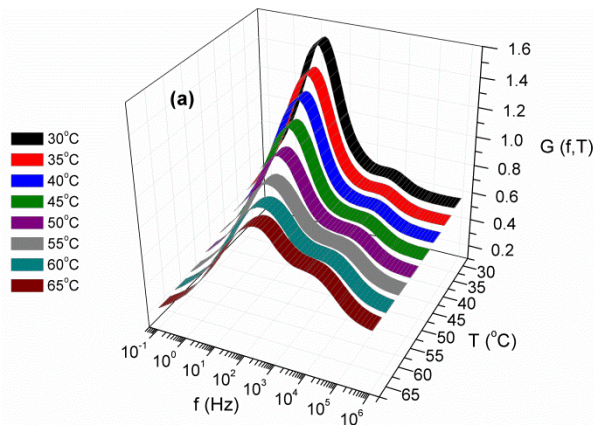
452

453 
$$G(f, T) = \frac{\varepsilon'_{comp}(f, T)}{\varepsilon'_{mat}(f, T)} \quad (7)$$

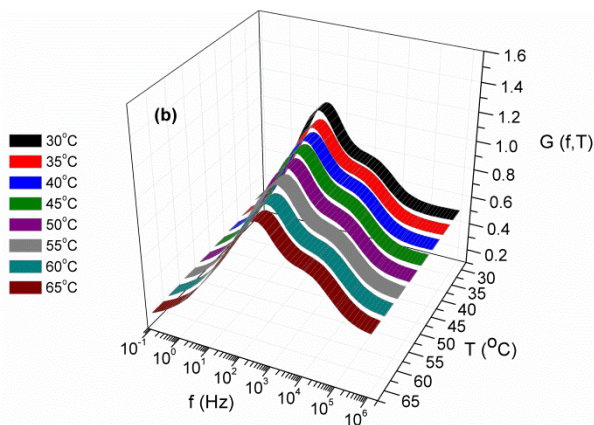
454

455 where  $\varepsilon'_{comp}(f, T)$  and  $\varepsilon'_{mat}(f, T)$  is the real part of dielectric permittivity of the  
 456 composite and the matrix respectively, while  $f$  is the frequency of the field and  $T$  the  
 457 temperature (Ioannou, Patsidis, & Psarras, 2011). It should be noted that TPS is  
 458 considered as the matrix. DRF is a dimensionless function being a measure of the  
 459 normalized polarization, upon the geometrical characteristics of the samples, and the  
 460 dielectric strengthening ability of the modifier. Additionally, DRF offers a strong  
 461 indication relative to the energy storing efficiency of the composites (Ioannou et al.,  
 462 2011; Patsidis, & Psarras, 2013).

463



464



465 **Fig. 5:** DRF as a function of frequency and temperature for TPS + 10% Latex for the:  
 466 (a) first and (b) second thermal cycle.

467

468 Fig. 5 presents the variation of DRF with temperature and frequency for TPS + 10%  
469 Latex. Fig. 5a shows the first thermal cycle where two processes are recorded. There  
470 is one peak at low to medium frequencies, which is indicative of the existence of  
471 water and also another process at higher frequencies which indicates  $\alpha$ -relaxation. As  
472 the temperature rises, DRF values for the water-related peak fall and stabilize at 60  
473 and 65°C, when all water is assumed as evaporated. The remaining peak could be  
474 attributed to interfacial polarization between the composite's constituents and  
475 possibly to a trapped limited quantity of water. In the second thermal cycle, as Fig.  
476 5b shows, the DRF values for the water-related peak are stable in the whole  
477 temperature range, since water has been evaporated, and thus only the interfacial  
478 phenomena are at work. The DRF values for  $\alpha$ -relaxation in Fig. 5a differ only at  
479 lower temperatures, compared to Fig. 5b, as water molecules slightly affect the  $\alpha$ -  
480 mode. Limited quantity of water molecules absorbed by the TPS matrix evaporate by  
481 heating leading to a variation of the Vogel temperature (Table 2).

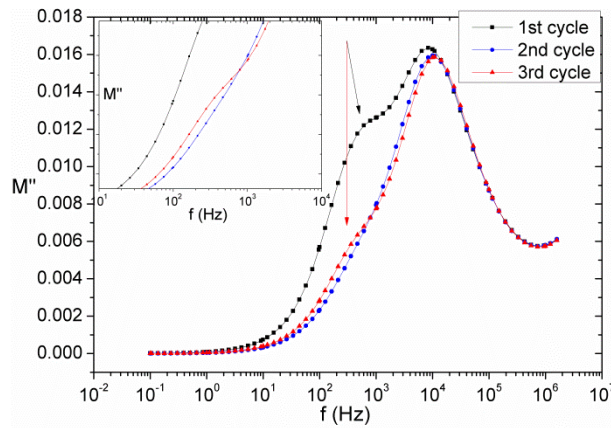
482

### 483 3.4. *Environmental exposure*

484 Fig. 6 presents the imaginary part of electric modulus as a function of frequency at  
485 30°C for the TPS + 20% B600 sample. After the second thermal cycle, the specimen  
486 was exposed to ambient temperature and humidity conditions for 120 hours prior to a  
487 third testing cycle. The third thermal cycle shows that part of the adsorbed water was  
488 retrieved during the environmental exposure. The loss peak at  $10^2$  Hz indicates the  
489 existence of that water. This peak is evident in the spectra of the first cycle and the  
490 third thermal cycles. In the first one the high water concentration results from the  
491 specimen's manufacturing process, while in the third cycle retrieved water originates



492 from the environmental exposure. Obviously, this peak is absent in the spectrum of  
493 the second thermal cycle, since water has been evaporated.



494

495 **Fig. 6:** Imaginary part of electric modulus as a function of frequency at 30°C for TPS  
496 + 20% B600 for the first, the second and the third thermal cycle.

497

498

#### 499 **4. Conclusion**

500 The effect of water on the dielectric properties and electrical conductivity of  
501 thermoplastic starch (TPS) modified with microfibrillated cellulose and natural rubber  
502 latex microparticles was investigated in the present study. Dielectric permittivity  
503 increases with frequency decrement, temperature rise and cellulose content. Electric  
504 modulus loss spectra during the first thermal cycle indicate the presence of two  
505 relaxation processes, which are attributed to MWR-IP and glass to rubber transition  
506 ( $\alpha$ -relaxation). MWR-IP relaxation process is assigned to the existence of water  
507 molecules between the polymer chains and constituents. This relaxation process  
508 diminishes as temperature rise until all water is evaporated. Relaxation dynamics of  $\alpha$ -  
509 mode process appear to be weakly affected at low temperatures from water content.  
510 Energy density increases as frequency falls and also during water evaporation. The  
511 influence of temperature is very important on water content. Hence, the dielectric

512 behavior of the specimens varies according to the filler's nature (hydrophilic or  
513 hydrophobic) and concentration, as well as the sample's treatment. Finally, it was  
514 observed that evaporated water can be partially retrieved inside the composites, under  
515 proper environmental conditions, indicating that the effect of absorption/evaporation  
516 is reversed. Hence, TPS biocomposites modified with microfibrillated cellulose and  
517 latex microparticles could be considered as functional materials exhibiting sensing  
518 capabilities.

519

## 520 **Acknowledgement**

521 The work reported here was supported by the Hungarian Research Fund (OTKA)  
522 through the project K 109409.

523

## 524 **References**

525

526 Arous, M., Ben Amor I., Boufi, S., & Kallel, A. (2007). Experimental study on  
527 dielectric relaxation in alfa fiber reinforced epoxy composites. *Journal of Applied*  
528 *Polymer Science*, 106, 3631-3640.

529 Bugnicourt, E., Cinelli, P., Lazzeri, A., & Alvarez, V. (2014). Polyhydroxyalkanoate  
530 (PHA): Review of synthesis, characteristics, processing and potential applications in  
531 packaging. *Express Polymer Letters*, 8, 791-808.

532 Chen, B., & Evans, J. R. G. (2005). Thermoplastic starch-clay nanocomposites and  
533 their characteristics. *Carbohydrate Polymers*, 6, 455-463.

534 Chung, Y.-L., Ansari, S., Estevez, L., Hayrapetyan, S., Giannelis, E. P., & Lai, H.-M.  
535 (2010). Preparation and properties of biodegradable starch-clay nanocomposites.  
536 *Carbohydrate Polymers*, 79, 391-396.

537 Dean, K., Yu, L., & Wu, D. Y. (2007). Preparation and characterization of melt-  
538 extruded thermoplastic starch/clay nanocomposites. *Composites Science and*  
539 *Technology*, 67, 413-421.

540 Gatos, K. G., Martínez Alcázar, J. G., Psarras, G. C., Thomann, R., & Karger-Kocsis,  
541 J. (2007). Polyurethane latex/water dispersible boehmite alumina nanocomposites:  
542 Thermal, mechanical and dielectrical properties. *Composites Science and Technology*,  
543 67, 157-167.

544 Herculano, R. D., Silva, C. P., Ereno, C., Guimaraes, S. A. C., Kinoshita, A., &  
545 Graeff, C. F. O. (2009). Natural rubber latex used as drug delivery system in guided  
546 bone regeneration (GBR). *Materials Research*, 12, 253-256.

547 Ioannou, G., Patsidis, A., & Psarras, G. C. (2011). Dielectric and functional properties  
548 of polymer matrix/ZnO/BaTiO<sub>3</sub> hybrid composites. *Composites: Part A: Applied*  
549 *Science and Manufacturing*, 42, 104-110.

550 Iqbal, H. M. N., Kyazze, G., Locke, I. C., Tron, T., & Keshavarz, T. (2015).  
551 Development of novel antibacterial active, HaCaT biocompatible and biodegradable  
552 CA-g-P(3HB)-EC biocomposites with caffeic acid as a functional entity. *Express*  
553 *Polymer Letters*, 9, 764-772.

554 Kamel S. (2007). Nanotechnology and its applications in lignocellulosic composites, a  
555 mini review. *Express Polymer Letters*, 1, 546-575.

556 Karger-Kocsis, J., Kmetty, Á., Lendvai, L., Drakopoulos, S. X., & Bárány, T. (2015).  
557 Water-assisted production of thermoplastic nanocomposites: A review. *Materials*, 8,  
558 72-95.

559 Kmetty, Á., Karger-Kocsis, J., & Czigány, T. (2015). Production and properties of  
560 micro-cellulose reinforced thermoplastic starch. *IOP Conference Series: Materials*  
561 *Science and Engineering*, 74, 012008.

562 Kremer F., & Schönhals A. (2009). Broadband dielectric measurement techniques  
563 ( $10^{-6}$  Hz to  $10^{12}$  Hz). In F. Kremer, & A. Schönhals (Eds.), *Broadband dielectric*  
564 *spectroscopy* (pp. 35-64) Springer, Berlin.

565 Ladhar, A., Arous, M., Kaddami, H., Raihane, M., Kallel, A., Graça, M. P. F., et al.  
566 (2014). Molecular dynamics of nanocomposites natural rubber/cellulose nanowhiskers  
567 investigated by impedance spectroscopy. *Journal of Molecular Liquids*, *196*, 187-191.

568 Lendvai, L., Karger-Kocsis, J., Kmetty, Á., & Drakopoulos, S. X. (2016). Production  
569 and characterization of microfibrillated cellulose-reinforced thermoplastic starch  
570 composites. *Journal of Applied Polymer Science*, *133*, 42397.

571 Liu, H., Xie, F., Yu, L., Chen, L., & Li, L. (2009). Thermal processing of starch-based  
572 polymers. *Progress in Polymer Science*, *34*, 1348-1368.

573 Majdzadeh-Ardakani, K., Navarchian, A. H., & Sadeghi, F. (2010). Optimization of  
574 mechanical properties of thermoplastic starch/clay nanocomposites. *Carbohydrate*  
575 *Polymers*, *79*, 547-554.

576 Mano, J. F., Koniarova, D., & Reis, R. L. (2003). Thermal properties of thermoplastic  
577 starch/ synthetic polymer blends with potential biomedical applicability. *Journal of*  
578 *Materials Science: Materials in Medicine*, *14*, 127-135.

579 Nafchi, A. M., Moradpour, M., Saeidi, M., & Alias, A. K. (2013). Thermoplastic  
580 starches: Properties, challenges, and prospects. *Starch*, *65*, 61-72.

581 Nasser, R., & Mohammadi, N. (2014). Starch-based nanocomposites: A comparative  
582 performance study of cellulose whiskers and starch nanoparticles. *Carbohydrate*  
583 *Polymers*, *106*, 432-439.

584 Ortiz-Serna, P., Carsí, M., Redondo-Foj, B., & Sanchis, M. J. (2014). Electrical  
585 conductivity of natural rubber-cellulose II nanocomposites. *Journal of Non-*  
586 *Crystalline Solids*, *405*, 180-187.

587 Patsidis, A. C., & Psarras, G. C. (2013). Structural transition. dielectric properties and  
588 functionality in epoxy resin-barium titanate nanocomposites. *Smart Materials and*  
589 *Structures*, 22, 115006.

590 Psarras, G. C., Gatos, K. G., Karahaliou, P. K., Georga, S. N., Krontiras, C. A., &  
591 Karger-Kocsis J. (2007). Relaxation phenomena in rubber/layered silicate  
592 nanocomposites. *Express Polymer Letters*, 1, 837-845.

593 Psarras, G. C., Gatos, K. G., & Karger-Kocsis, J. (2007). Dielectric properties of  
594 layered silicate-reinforced natural and polyurethane rubber nanocomposites. *Journal of*  
595 *Applied Polymer Science*, 106, 1405-1411.

596 Rolere, S., Bottier, C., Vaysse, L., Sainte-Beuve, J., & Bonfils, F. (2016).  
597 Characterisation of macrogel composition from industrial natural rubber samples:  
598 Influence of proteins on the macrogel crosslink density. *Express Polymer Letters*, 10,  
599 408-419.

600 Rose K., & Steinbüchel A. (2005). Biodegradation of natural rubber and related  
601 compounds: Recent insights into a hardly understood catabolic capability of  
602 microorganisms. *Applied Environmental Microbiology*, 71, 2803-2812.

603 Ruellan, A., Guinault, A., Sollogoub, C., Chollet, G., Ait-Mada, A., Ducruet, V., et al.  
604 (2015). Industrial vegetable oil by-products increase the ductility of polylactide.  
605 *Express Polymer Letters*, 9, 1087-1103.

606 Schlemmer, D., Angélica, R. S., & Sales, M. J. A. (2010). Morphological and  
607 thermomechanical characterization of thermoplastic starch/montmorillonite  
608 nanocomposites. *Composite Structures*, 92, 2066-2070.

609 Siengchin, S., Karger-Kocsis, J., Psarras, G. C., & Thomann, R. (2008).  
610 Polyoxymethylene/polyurethane/alumina ternary composites: Structure, mechanical,

611 thermal and dielectric properties. *Journal of Applied Polymer Science*, 110, 1613-  
612 1623.

613 Siengchin, S., Karger-Kocsis, J., & Thomann, R. (2008). Nanofilled and/or toughened  
614 POM composites produced by water-mediated melt compounding: Structure and  
615 mechanical properties. *Express Polymer Letters*, 2, 746-756.

616 Tábi T., & Kovács J. G. (2007). Examination of injection moulded thermoplastic  
617 maize starch. *Express Polymer Letters*, 1, 804-809.

618 Tanrattanakul, V., & Bunkaew, P. (2014). Effect of different plasticizers on the  
619 properties of bio-based thermoplastic elastomer containing poly(lactic acid) and  
620 natural rubber. *Express Polymer Letters*, 8, 387-396.

621 Tsangaris, G. M., Psarras, G. C., & Kouloumbi, N. (1998). Electric modulus and  
622 interfacial polarization in composite polymeric systems. *Journal of Materials*  
623 *Science*, 33, 2027-2037.

624 Xie, F., Pollet, E., Halley, P. J., & Avérous, L. (2013). Starch-based nano-  
625 biocomposites. *Progress in Polymer Science*, 38, 1590-1628.

